



HAL
open science

Probing the antiferromagnetic-paramagnetic transition in artificial spin ice by tuning interactions

Maryam Massouras, Daniel Lacour, Michel Hehn, François Montaigne

► **To cite this version:**

Maryam Massouras, Daniel Lacour, Michel Hehn, François Montaigne. Probing the antiferromagnetic-paramagnetic transition in artificial spin ice by tuning interactions. *Physical Review B: Condensed Matter* (1978-1997), 2020, 101, 10.1103/PhysRevB.101.174421 . hal-02887697

HAL Id: hal-02887697

<https://hal.science/hal-02887697>


Submitted on 2 Jul 2020

HAL is a multi-disciplinary open access archive for the deposit and dissemination of scientific research documents, whether they are published or not. The documents may come from teaching and research institutions in France or abroad, or from public or private research centers.

L'archive ouverte pluridisciplinaire **HAL**, est destinée au dépôt et à la diffusion de documents scientifiques de niveau recherche, publiés ou non, émanant des établissements d'enseignement et de recherche français ou étrangers, des laboratoires publics ou privés.

Probing the antiferromagnetic-paramagnetic transition in artificial spin ice by tuning interactions

Maryam Massouras , Daniel Lacour , Michel Hehn , and François Montaigne ^{*}
Université de Lorraine, CNRS, Institut Jean Lamour, F-54000 Nancy, France

 (Received 30 January 2020; accepted 9 April 2020; published 14 May 2020)

Artificial spin ice systems, two-dimensional arrays of interacting nanomagnets, provide a playground to directly observe competing interactions. Due to the anisotropic nature of the dipolar interactions, rotation of nanomagnets is a powerful way of tuning the interactions. In this paper, we experimentally examine the ground state transition from antiferromagnetic to ferromagnetic order triggered by this transformation. The as-grown magnetic configurations well agree with Monte Carlo simulations and ascribe a unique effective temperature independent of the rotation angle. Deviations from the theoretical ground state and behavior at transition are therefore well explained.

DOI: [10.1103/PhysRevB.101.174421](https://doi.org/10.1103/PhysRevB.101.174421)

Artificial spin systems, generally referred to as artificial spin ice, are interesting realizations of nanomagnets interacting via dipolar magnetic coupling [1–3]. Offering the flexibility of top-down fabrication techniques and the precise determination of magnetic configurations by magnetic imaging [4–8], artificial spin systems constitute a wide playground for statistical physics and might offer application opportunities [9]. The properties of an artificial spin system depend obviously on both the geometry of the lattice [10,11] and the nature of the spin which is mainly an in-plane Ising-like spin (out-of-plane Ising spin systems [12] and Potts spin system [13] have also been demonstrated). Both aspects directly impact the interactions between spins but these interactions can be further tuned by modulation of elements heights [14] or rotation of the spins [15,16]. Such an angular rotation of the spins leads to a drastic evolution of properties from the square ice to the pinwheel lattice [15,17]. The square ice [Fig. 1(a)] was the first proposed artificial spin ice system [1]. The “spin ice” appellation originates from the dipolar interactions favoring two-in/two-out vertices similarly to bulk magnetic spin ice. This analogy is rather limited as the six pair interactions within a vertex are not equivalent. The degeneracy expected from the geometric frustration is therefore lifted and the ground state of the system is an antiferromagnetic configuration [18]. This configuration has been experimentally observed in “as-grown” samples [19] and then in the superparamagnetic regime [20,21]. The pinwheel lattice [Fig. 1(b)] is expected to have a ferromagnetic ground state. This ferromagnetic state has been observed by Li *et al.* and Gliga *et al.* [16,17] under field-driven reversal. The continuous transformation from the square ice lattice to the pinwheel lattice is achieved by rotation of the spins relatively to the square lattice. This transformation has been studied theoretically by Macêdo *et al.* [15]. The phase diagram of the system as a function of the rotation angle and temperature

shows the presence of three phases: paramagnetic at high temperature, antiferromagnetic for rotation angles below 35° , and ferromagnetic for angles above.

We examine a set of artificial spin ice systems composed by ten tilted networks with elements rotated around their midpoint of an angle ranging from 0° to 45° in steps of 5° . Rotation is shown in Figs. 1(a) and 1(b), from square ice with closed edges to pinwheel ice with diamond edges [15]. The nanomagnets are 400 nm long, 100 nm wide, spaced 500 nm, and have circular ends so they behave like Ising spins. Each array of 1800 elements was fabricated using electron beam lithography, evaporation to deposit 20-nm-thick Permalloy, followed by liftoff to ensure shape anisotropy. We observe the as-grown state, right after liftoff using magnetic force microscopy (MFM) as in Refs. [19,22].

The two extreme cases, square or 0° - and pinwheel or 45° -tilted networks, are shown in Figs. 1(a) and 1(b). The square array observed by MFM in Fig. 1(c) reveals a perfect checkerboard arrangement with exclusively type 1 vertices on its vertex population as shown in Fig. 2(b). Thus we confirm the long-range ground state of our as-grown system like in Ref. [19]. The 45° -tilted array observed by MFM in Fig. 1(d) shows large ferromagnetic domains and its vertex population a majority of type 2 vertices. The two tilings experimentally confirm the transition from antiferromagnetic to ferromagnetic ground state due to tuning of the interactions by element rotation.

We use the magnetic structure factor and vertex population to determine the order of each array shown in Figs. 2(b) and 2(c). We identify two states depending on the rotation angle. On one hand, tilings with rotation angle up to 25° exhibit two features: more than 90% of vertex population consisting of type 1 vertices and same pattern on the magnetic structure factor as the square geometry. Focusing on the 25° -tilted array, its magnetic structure factor in Fig. 3(a)ii, exhibits sharp Bragg peaks located at the corners of the Brillouin zone specific of antiferromagnetic order. Its spin configuration in Fig. 3(a)i shows a large antiferromagnetic domain (in green), a small domain of the other configuration (in black), and few spins flipped. These excitations respectively creating a domain

^{*}francois.montaigne@univ-lorraine.fr

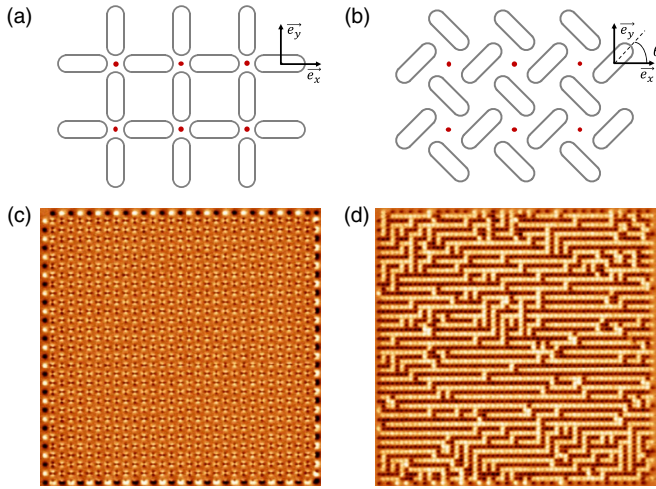


FIG. 1. (a) Square ice or $\theta = 0^\circ$ and (b) pinwheel ice or $\theta = 45^\circ$ lattice arrangements. (c) Observation of square and (d) 45° -tilted networks as-grown state using MFM.

wall of type 2 vertices and monopole-antimonopole pairs [6] have no consequence on the antiferromagnetic state expected from dipolar coupling as seen on the magnetic structure factor.

On the other hand, decreasing the rotation angle of the array from 45° to 40° does not change the Bragg peaks on magnetic structure factor or the prevalence of type 2 on vertex populations as shown in Figs. 2(b) and 2(c). As highlighted in Figs. 3(d)i and 3(d)ii, the 40° -tilted tiling shows Bragg peaks on magnetic structure factor located at the center of the Brillouin zones specific of ferromagnetic order. Its spin configuration shows ferromagnetic domains that are of different configurations and although domain walls are created, the tiling still exhibits a clear ferromagnetic state.

We experimentally demonstrated the transition from antiferromagnetic order for rotation angles up to 25° to ferromagnetic order for angles higher than 40° . However for rotation angles in between, the cross sections on magnetic structure factor Fig. 2(c) reveal Bragg peaks of both antiferromagnetic and ferromagnetic orders suggesting a coexistence of both states which is highlighted in Figs. 3(b)ii and 3(c)ii. The 30° tiling has 49% of its vertices that are of type 1, 28% of type 2, and 23% of type 3 [Fig. 2(b)]. The type 1 vertices form antiferromagnetic domains of both configurations (green and black ensembles) separated by domain walls of type 2 and 3 vertices as shown in Fig. 3(b)i. These two features account for the antiferromagnetic and ferromagnetic Bragg peaks on the magnetic structure factor, respectively. However, the 35° tiling has 21% of its vertices that are of type 1, 48% of type 2, and 31% of type 3 translating in spin configuration in small ferromagnetic domains and numerous smaller antiferromagnetic domains. Both features are responsible for the antiferromagnetic and ferromagnetic Bragg peaks on magnetic structure factor.

We have seen that tilting our arrays induces a change from antiferromagnetic to ferromagnetic order, and in between a coexistence of both. To better understand how our system behaves, we compute its dipolar energy using the following

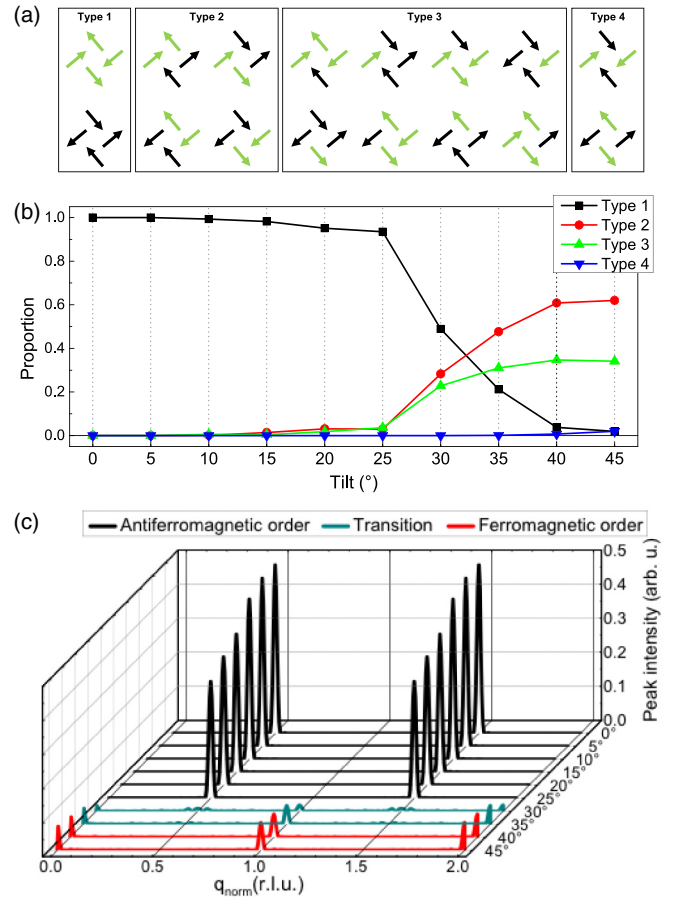


FIG. 2. (a) The 16 possible vertices: types 1, 2 two-in/two-out configurations specific of antiferromagnetic and ferromagnetic orders, respectively; types 3, 4 single and double monopole-charged configurations. Green and black colors indicate the two possible type 1 or antiferromagnetic configurations. (b) Vertex populations of our system and (c) its cross sections on the magnetic structure factor along the diagonal.

Hamiltonian:

$$\mathcal{H}_{\text{dip}} = Da^3 \sum_{i \neq j} \left[\frac{\vec{S}_i \cdot \vec{S}_j}{r_{ij}^3} - \frac{3(\vec{S}_i \cdot \vec{r}_{ij})(\vec{S}_j \cdot \vec{r}_{ij})}{r_{ij}^5} \right], \quad (1)$$

where $D = \mu_0 \mu^2 / 4\pi a^3$ is the dipolar coupling constant, a the lattice spacing, and $r_{ij}^2 = [\vec{e}_x \cdot (\vec{r}_i - \vec{r}_j)]^2 + [\vec{e}_y \cdot (\vec{r}_i - \vec{r}_j)]^2$ the distance between spins i and j . The energy calculated for experimental configurations is represented in Fig. 4 and first compared to the energy of the two simple ground states: antiferromagnetic (black dashed line) and ferromagnetic (red dashed line). For the latter, we consider a Landau configuration that is the lower energy state for a finite square system [15]. For rotation angles between 0° and 25° , the experimental energy is close to the ground state in agreement with the nearly perfect antiferromagnetic order observed. Between 30° and 45° , the experimental energy deviates significantly with respect to the ground state. This tendency is expected as the coupling coefficients decrease with the angle and the energy difference between different configurations also globally decreases. In order to possibly ascribe an effective tempera-

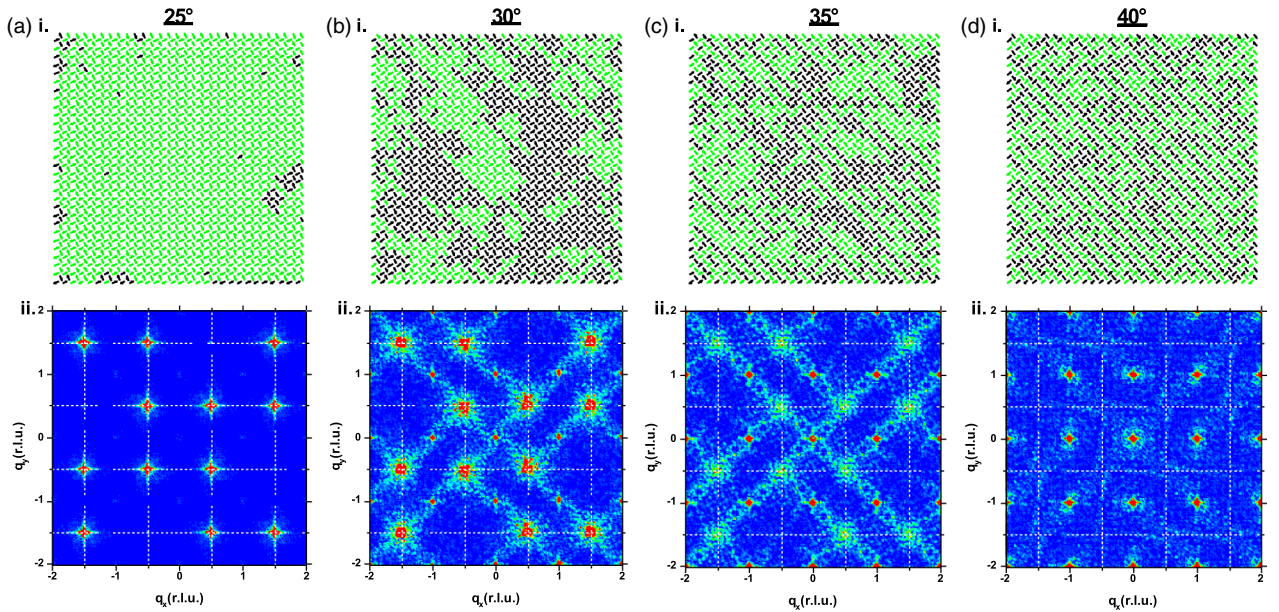


FIG. 3. Spin configurations and magnetic structure map of (a)i and (a)ii, 25°-tilted network exhibiting antiferromagnetic order; (b) and (b)ii, 30°-tilted; (c) i and (c)ii, 35°-tilted network exhibiting both orders coexisting; and (d)i and (d)ii, 40°-tilted network exhibiting ferromagnetic order.

ture to our system, it is necessary to quantitatively compare the experimental configurations with equilibrium properties of the theoretical system. Therefore, we performed Monte Carlo Metropolis simulations on a system size identical to the experimental one taking all interactions into consideration. Equilibrium energies deduced from simulations as a function of the system angle for three different temperatures are represented in Fig. 4. It appears that the experimental energies are compatible with an effective temperature of $k_B T_{\text{eff}} = 2.8D$. For comparison, this temperature can also be

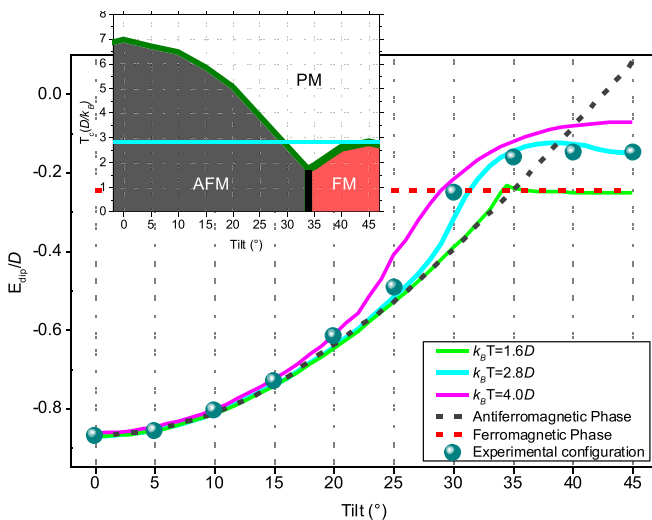


FIG. 4. Dipolar energy of our experimental system compared to antiferromagnetic and ferromagnetic phases with interactions minimized all over the array (dashed lines) and computed effective temperatures using Monte Carlo simulations (solid lines). The inset shows the phase diagram of our system based on the same method as Macêdo *et al.* [15].

expressed relatively to $E_3 - E_1$ [23,24], the energy difference between type 3 and type 1 vertices for the square geometry. As in the dipolar approximation $E_3 - E_1 = 4(3\sqrt{2} - 1)D$, $(E_3 - E_1)/(k_B T_{\text{eff}}) = 4.6$. Remarkably, a single temperature describes the different geometries. We emphasize that considering all the interactions is essential to achieve this result. The 16 vertex model [23,24] cannot account for the observed features; especially for the 45°-tilted array, since the interaction between first nearest neighbors is null, longer range interactions are needed. Even for the classical square geometry, both models differ significantly. In our case, for the effective temperature $k_B T_{\text{eff}} = 2.8D$, the system lies in its ground state (100% of type 1 vertices), whereas a significant number of excitations is expected within the 16 vertex model (89% of type 1 vertices, 7% of type 2, and 3% of type 3). Note that for a field-driven demagnetization (oscillatory sinusoidal field with an amplitude decreased by 3.3 Oe per period), it is not possible to affect a unique effective temperature for the whole angular range. We established the phase diagram of our system based on the same method as Macêdo *et al.* [15] and compare it to our effective temperature in the inset of Fig. 4. It appears that the experimental configuration observed at 30° is not an antiferromagnetic-ferromagnetic transition but rather an antiferromagnetic-paramagnetic transition. At this transition, large antiferromagnetic domains (type 1) break up in small domains. Considering the uncertainty on the effective temperature and the possible deviations from the calculated phase diagram (due to finite size effects or inaccuracies of the dipolar approximation), it is not possible to conclude about the 40°- and 45°-tilted configurations. Their magnetic structure factors correspond to a ferromagnetic state but might nevertheless belong to the paramagnetic phase due to the continuous nature of the phase transition. The 35°-tilted array belongs to the paramagnetic phase, whereas the expected ground state for this angle is

ferromagnetic, small antiferromagnetic domains emerge as excitation from the ground state directly observed in the magnetic configurations.

The transition from the square artificial spin ice to the pinwheel lattice has been investigated by rotation of elementary spins. As expected from theoretical calculations, the system evolves from an antiferromagnetic state to a ferromagnetic state as spins are rotated. The experimental transitions are not abrupt and the two states coexist within a certain angular range. It is shown that the observed as-grown states are not the ground states of the system but are compatible with equilibrium states corresponding to an effective temperature of $2.8D$. This study illustrates that the

modulation in orientation of artificial spins is a powerful way to tune the dipolar interactions and realize new magnetic phases.

Note added. Recently we became aware of a recent related experimental work on the same system [25].

Nanofabrication was performed thanks to the technical support of G. Lengaigne and L. Badie. We acknowledge financial support from the impact project LUE-N4S part of the French PIA project “Lorraine Université d’Excellence”, Région Grand-Est and from the European Union program “FEDER-FSE Lorraine et Massif des Vosges 2014-2020” through the RaNGE project.

-
- [1] R. F. Wang, C. Nisoli, R. S. Freitas, J. Li, W. McConville, B. J. Cooley, M. S. Lund, N. Samarth, C. Leighton, V. H. Crespi, and P. Schiffer, *Nature (London)* **439**, 303 (2006).
- [2] L. J. Heyderman and R. L. Stamps, *J. Phys.: Condens. Matter* **25**, 363201 (2013).
- [3] J. Cumings, L. J. Heyderman, C. H. Marrows, and R. L. Stamps, *New J. Phys.* **16**, 075016 (2014).
- [4] S. Ladak, D. E. Read, G. K. Perkins, L. F. Cohen, and W. R. Branford, *Nat. Phys.* **6**, 359 (2010).
- [5] E. Mengotti, L. J. Heyderman, A. Fraile Rodríguez, A. Bisig, L. Le Guyader, F. Nolting, and H. B. Braun, *Phys. Rev. B* **78**, 144402 (2008).
- [6] E. Mengotti, L. J. Heyderman, A. F. Rodríguez, F. Nolting, R. V. Hügli, and H.-B. Braun, *Nat. Phys.* **7**, 68 (2011).
- [7] Yi Qi, T. Brintlinger, and John Cumings, *Phys. Rev. B* **77**, 094418 (2008).
- [8] D. J. P. Morris, D. A. Tennant, S. A. Grigera, B. Klemke, C. Castelnovo, R. Moessner, C. Czternasty, M. Meissner, K. C. Rule, J.-U. Hoffmann, K. Kiefer, S. Gerischer, D. Slobinsky, and R. S. Perry, *Science* **326**, 411 (2009).
- [9] J. H. Jensen, E. Folven, and G. Tufte, in *The 2018 Conference on Artificial Life: A Hybrid of the European Conference on Artificial Life (ECAL) and the International Conference on the Synthesis and Simulation of Living Systems (ALIFE)*, edited by T. Ikegami, N. Virgo, O. Witkowski, M. Oka, R. Suzuki, and H. Iizuka (Massachusetts Institute of Technology, 2018), pp. 15–22.
- [10] M. J. Morrison, T. R. Nelson, and C. Nisoli, *New J. Phys.* **15**, 045009 (2013).
- [11] F. Montaigne, D. Lacour, I. A. Chioar, N. Rougemaille, D. Louis, S. M. Murtry, H. Riahi, B. Santos Burgos, T. O. Menten, A. Locatelli, B. Canals, and M. Hehn, *Sci. Rep.* **4**, 5702 (2015).
- [12] I. A. Chioar, N. Rougemaille, A. Grimm, O. Fruchart, E. Wagner, M. Hehn, D. Lacour, F. Montaigne, and B. Canals, *Phys. Rev. B* **90**, 064411 (2014).
- [13] D. Louis, D. Lacour, M. Hehn, V. Lomakin, T. Hauet, and F. Montaigne, *Nat. Mater.* **17**, 1076 (2018).
- [14] Y. Perrin, B. Canals, and N. Rougemaille, *Nature (London)* **540**, 410 (2016).
- [15] R. Macêdo, G. M. Macauley, F. S. Nascimento, and R. L. Stamps, *Phys. Rev. B* **98**, 014437 (2018).
- [16] Y. Li, G. W. Paterson, G. M. Macauley, F. S. Nascimento, C. Ferguson, S. A. Morley, M. C. Rosamond, E. H. Linfield, D. A. MacLaren, R. Macêdo, C. H. Marrows, S. McVitie, and R. L. Stamps, *ACS Nano* **13**, 2213 (2019).
- [17] S. Gliga, G. Hrkac, C. Donnelly, J. Büchi, A. Kleibert, J. Cui, A. Farhan, E. Kirk, R. V. Chopdekar, Y. Masaki, N. S. Bingham, A. Scholl, R. L. Stamps, and L. J. Heyderman, *Nat. Mater.* **16**, 1106 (2017).
- [18] L. A. S. Mól, W. A. Moura-Melo, and A. R. Pereira, *Phys. Rev. B* **82**, 054434 (2010).
- [19] J. P. Morgan, A. Stein, S. Langridge, and C. H. Marrows, *Nat. Phys.* **7**, 75 (2011).
- [20] A. Farhan, P. M. Derlet, A. Kleibert, A. Balan, R. V. Chopdekar, M. Wyss, J. Perron, A. Scholl, F. Nolting, and L. J. Heyderman, *Phys. Rev. Lett.* **111**, 057204 (2013).
- [21] O. Sendetskyi, V. Scagnoli, N. Leo, L. Anghinolfi, A. Alberca, J. Lüning, U. Staub, P. M. Derlet, and L. J. Heyderman, *Phys. Rev. B* **99**, 214430 (2019).
- [22] C. Nisoli, *New J. Phys.* **14**, 035017 (2012).
- [23] C. Nisoli, J. Li, X. Ke, D. Garand, P. Schiffer, and V. H. Crespi, *Phys. Rev. Lett.* **105**, 047205 (2010).
- [24] J. P. Morgan, J. Akerman, A. Stein, C. Phatak, R. M. L. Evans, S. Langridge, and C. H. Marrows, *Phys. Rev. B* **87**, 024405 (2013).
- [25] G. M. Macauley, G. W. Paterson, Y. Li, R. Macêdo, S. McVitie, and R. L. Stamps, *Phys. Rev. B* **101**, 144403 (2020).